2021 43rd Annual International Conference of the
IEEE Engineering in Medicine & Biology Society (EMBC)
Oct 31 - Nov 4, 2021. Virtual Conference

Deep Learned Super Resolution of System Matrices for Magnetic Particle Imaging

Alper Güngör[1,2], Baris Askin[1], Damla Alptekin Soydan[2,3], Can Barış Top[2], Tolga Cukur[1]

Abstract— **Magnetic Particle Imaging (MPI) is a new imaging technique that allows high resolution & high frame-rate imaging of magnetic nanoparticles (MNP). It relies on the non-linear response of MNPs under a magnetic field. The imaging process can be modeled linearly, and then image reconstruction can be case as an inverse problem using a measured system matrix (SM). However, this calibration measurement is time consuming so it reduces practicality. In this study, we proposed a novel method for accelerating the SM calibration based on joint super-resolution (SR) and denoising of sensitivty maps (i.e., rows of SM). The proposed method is based on a deep convolutional neural network (CNN) architecture with residual-dense blocks. Model training was performed using noisy SM measurements simulated for varying MNP size and gradient strengths. Comparisons were performed against conventional low-resolution SM calibration, noisy high-resolution SM calibration, and bicubic upsampling of low-resolution SM. We show that the proposed method improves high-resolution SM recovery, and in turn leads to improved resolution and quality in subsequently reconstructed MPI images.**

I. Introduction

Magnetic Particle Imaging (MPI) is a recent modality that allows imaging the distribution of magnetic nanoparticle (MNP tracers) based on their non-linear magnetization response [1]. MPI is amenable to real-time imaging as it can achieve high frame-rates [2]. These properties render it an ideal modality for applications such as stem cell tracking, angiography and targeted drug delivery [3]–[5]. To image MNP tracers, MPI first exerts a non-homogeneous static magnetic field (i.e., *selection field*) with a field of view (FOV). The (SF) contains a field free region (FFR) that can be a single point (FFP, field-free point) or a single line (FFL, field-free line). A time-varying *drive field* is then applied to reposition the FFR across the FOV. MNPs within FFR are responsive whereas those outside yield no response due to saturation. Therefore, the MPI signal consists of the nonlinear responses of MNPs within FFR at the drive field frequency and its harmonics, which is generally acquired using receive coil(s). In this study, we consider system matrix (SM) based image reconstruction for MPI [1]. SM-based method case an inverse problem where the the measured SM linearly projects the image onto the measured signals. To measure SM, a small MNP sample is imaged while its location is systematically altered across the FOV. SM-based reconstructions can offer improved image quality as they can account for non-ideal response of MNPs and coils that generate magnetic fields [6]. However, a priori measurement of SM results in excessive calibration times. For a typical FOV of $32\times32\times32$ voxels and 1.3 sec acquisition time per sample, an astounding 12 hours are required for full calibration [7]. Note that SM is specific to the imaging setup, and recalibration is needed with changes to the system configuration of FFL scan trajectory [8]. Therefore, there is a dire need for scan-efficient calibration procedures.

To accelerate SM calibration, previous studies have proposed compressed sensing (CS) methods [9], [10]. Rows of SM correspond to spatial sensitivity maps of the MPI system. CS methods collect a random subset of SM measurements, and recover the full SM by enforcing sparsity in discrete cosine or Chebyshev transform domains. While CS methods have been reported to enable moderate accelerations (around 10-fold [11]), iterative optimization procedures involve substantial computational burden, and large FOVs typically prescribed in clinical scans necessitate further acceleration of the calibration procedure. Furthermore, a recent study have proposed using simulated SM, as well as the experimentally measured SM for joint estimation of both the underlying MPI image and the SM [12]. This method requires a simulated SM of the experimental system for reconstruction. Moreover, the computational burden of the reconstruction procedure increases significantly, since both SM and the image is recovered simultaneously, for each image.

Here we introduce a deep-learning approach for simultaneous super-resolution (SR) and denoising to capture high-resolution (HR) SM with short calibration times. While SR techniques typically aim to increase resolution in image domain, MNP distribution across the FOV is difficult to model in MPI. Instead, we resolve sensitivity maps of the coils that are properties of intact physical systems and easier to model. Given the success of convolutional neural networks (CNNs) in SR tasks for computer vision, we adopt a deep-learning model based on CNNs [13]–[15]. Note, however, that MPI data are substantially smaller in size and they are complex-valued. Therefore, we proposed a CNN model adapted to MPI data. Accordingly, our contributions are as follows: 1) We proposed a CNN model for joint SR and denoising of system matrices. 2) We leverage an in-house MPI simulator to generate training data. 3) We compare the proposed learning-based method against SR based on linear interpolation [16]. 4) We show that the proposed method outperforms conventional methods visualy and quantitatively in SM recovery, and in subsequent image reconstruction tasks.

[1] Electrical and Electronics Eng. Dept., Bilkent University, Ankara, Turkey
[2] Aselsan Research Center, Ankara, Turkey
[3] Electrical and Electronics Eng. Dept., Middle East Technical University, Ankara, Turkey
Corresponding author: alpergungor@aselsan.com.tr

II. Background

A. Forward Model and Calibration Process

In MPI, a drive coil excites MNPs at a specific frequency, while a receiver coil samples the signal from the excited FOV. The received signal reflects high-intensity responses only in small bands centered at the harmonic frequencies. Hence, the signal can be compressed by filtering the harmonics in Fourier domain. The resulting signal model can be expressed as:

$$\mathbf{A}\mathbf{x} + \mathbf{n} = \mathbf{y}, \tag{1}$$

where $\mathbf{A} \in C^{M \times N}$, $\mathbf{x} \in R^N$, $\mathbf{y} \in C^M$ and $\mathbf{n} \in C^M$ represent the complex-valued SM, real-valued image vector, complex-valued data vector, and noise, respectively. M is the number of data points, while N is the number of grid points. We employ an FFL scanning MPI system in this study. Each row of $\mathbf{A}^{(i)} \in C^{1 \times N}$ corresponds to sensitivity map of the MPI scanner for i^{th} frequency / angle component.

In practice, the system matrix can show nonidealities due to coil hearing or inter-batch variations in MNP response [8]. A common solution this to perform a calibration scan where the system matrix is measured using a small MNP sample [7]. To capture SM, the sample is mechanically traversed across the entire FOV. The calibration measurements result in a noisy estimate of the SM:

$$\tilde{\mathbf{A}} = \mathbf{A} + \tilde{\mathbf{N}}, \tag{2}$$

$\tilde{\mathbf{N}}$ denotes additive noise, and $\tilde{\mathbf{A}}$ denotes the measured system matrix. Unfortunately, this calibration process can last several hours or even days, and it must be repeated across time due to drifts in imaging conditions. Note that the calibration MNP sample inherently determines the spatial resolution, where aiming for higher resolution leads to lower signal-to-noise ratio, which further prolongs the scan time. Therefore, a HR SM calibration will last substantially longer than a low-resolution (LR) SM calibration to maintain similar SNR. Moreover, signal intensity decreases with increasing frequency, which results in lower SNR in higher harmonics [17]. Finally, higher harmonics have more complex shapes compared to lower ones, which affects the SR performance [17].

B. Super-Resolution Methods

Single image super-resolution (SISR) is an open problem in the literature. Recently, deep learning based methods have gained attraction due to their success in computer vision tasks. Previous studies have focused mainly on capturing fine details as the super-resolution factor is increased. Ledig et al. have proposed using generative adversarial networks (GAN) with both pixel and perception loss to capture higher frequency details [13]. Soh et al. have proposed a technique to improve perceived image quality by using domain prior properties through constraining the output image to the natural manifold [14]. Zhang et al. have proposed using residual-dense network (RDN) with ℓ_1-norm loss that allows direct connections from low-resolution image to output for better utilization of low-resolution information in the final output image [15].

C. Image Reconstruction

MPI reconstruction can be cast as an inverse problem with the following optimization formulation [6]:

$$\arg\min_{\mathbf{x}} \ \alpha\|\mathbf{x}\|_1 + (1-\alpha)TV(\mathbf{x}) \text{s.t.} \|\mathbf{A}\mathbf{x} - \mathbf{y}\|_2 \leq \epsilon, \tag{3}$$

where ϵ is the bound on the ℓ_2-norm of noise, $TV(\cdot)$ is the total variation (TV) function that promotes gradient sparsity, and α is the trade-off parameter between TV and ℓ_1-norm. Choosing higher α results in sparser images, while TV promotes larger components in the image. Because we use measured noisy system matrix instead of the underlying system matrix, ϵ should be chosen to reflect potential mismatch between the underlying SM and the used SM, as well as the noise on the data. Here we used an alternating direction method of multipliers (ADMM) based algorithm for solving Eq. (3), where ADMM perform iterative optimization via splitting Eq. (3) into easier subproblems [6], [17].

In this study, we set the step size of ADMM small to assure convergence. We chose α value separately for each method to optimize the image quality in terms of peak signal to noise ratio (pSNR). We set ϵ to its optimal value which also accounts for the mismatch between the used SM and the reference SM, i.e. $\epsilon = \|\mathbf{A}\mathbf{x}_{ref} - \mathbf{y}\|$.

III. Methods

A. Proposed Super-Resolution Method

This study presents an MPI super-resolution technique based on upsampling of the MPI SM. Specifically, we propose a CNN based super-resolution method to estimate HR SMs from LR SM measurements. This approach will have two main advantages: enhanced SNR efficiency during calibration measurements at LR, and shortened calibration time due to fewer number of measurements. The super-resolution of SM can be formulated as:

$$\mathbf{A}^{(i)}_{CNN} = f_\theta\left(\mathbf{A}^{(i)}_{LR} + \tilde{N}^{(i)}\right). \tag{4}$$

Here, $f_\theta(\cdot)$ represents the CNN based estimator to be trained. In this study, we trained a single super-resolution network for all frequency / angle components i. Because MPI images usually have much smaller dimensions compared to visual images, we propose using a relatively compact network architecture with fewer parameters. Another key difference is that, MPI SM sensitivity maps are complex-valued. The real and imaginary components of SM rows were fed as separate inputs to the network, and the outputs were combined.

In this study, we proposed a deep super-resolution network that is comprised of Residual Dense Blocks (RDB) of "Residual Dense Network" (RDN) [15]. Residual and dense connections improve information flow across the network. RDBs are comprised of multiple inner densely connected convolutional layers, which increase the number of features. Moreover, each RDB has a residual connection from its input to output. The final inner layer concatenates the additional

features through a 1×1 convolutional layer to keep the input and output feature size of the RDB the same. To attain a compact network, 16 features and 4 inner layers within each RDB block were included with 4 RDBs. An ℓ_1-norm loss between the network estimate for HR SM and the true HR SM was used for training. Training details are presented in the following section.

B. Training

To generate the training set, we simulated an FFL-MPI system that images a 32×32 mm^2 FOV with 6 degrees-steps. During the simulations, we used MNPs with $0.55\ \mu_0/A/m$ magnetic saturation and $300°K$. SF gradient strength and MNP size were chosen as free parameters. SF was varied between 0.4 T/m to 1 T/m, while MNP size was varied between 14 nm and 33 nm. We simulated a sinusoidal drive field of 26 kHz for a period of 1 ms. Drive field strength was adapted to scan the whole FOV for the given SF strength. The relationship between particle magnetization and the applied magnetic field was represented using Langevin function [18]. The received signal was sampled using 2 MS/s sampling rate, and only the center frequencies of 2nd to 9th harmonics were used. In this study, we tried to resolve 32×32 (1 mm / pixel) images from 8×8 (4 mm / pixel) measured SMs.

Using various values of MNP size and SF strength, we generated 100 different SMs. Each SM consists of 8 frequency components, 30 angle components and a real and imaginary parts (a total of 480 sensitivity maps). We separated SMs generated with SF strength equal to 1 T/m up front as the test set, along with randomly selected SMs. We assumed a 30 dB SNR level with white Gaussian noise for the SM measurements, based on previous experiments conducted via our inhouse MPI system [17]. The noise-added system matrix elements were normalized to span from 0.15 to 0.85 to improve numerical stability in the SR network.

The network was implemented in PyTorch. At each epoch during network training, we used different noise realizations to improve robustness to noise. We trained the network for 500 epochs. We used ADAM optimizer with 8×10^{-3} learning rate, and 10^{-4} weight decay. For quantitative comparison of SM estimation performance, we used nRMSE defined as:

$$nRMSE = \|\mathbf{A} - \mathbf{A}_{ref}\|_F / \|\mathbf{A}_{ref}\|_F. \qquad (5)$$

We also implemented the image reconstruction algorithm using PyTorch library. For quantitative comparison of image reconstruction performance, we used pSNR and structural similarity index measure (SSIM) metrics.

IV. Results

To determine the proper model complexity for the MPI SM super-resolution task, we first built models of varying numbers of parameters by changing the number of RDN feature growth-rate in the network. Optimal model complexity was selected via k-fold cross validation with 5-folds. SM estimation performance (nRMSE) as a function of model complexity is illustrated in Fig. 1. As can be seen,

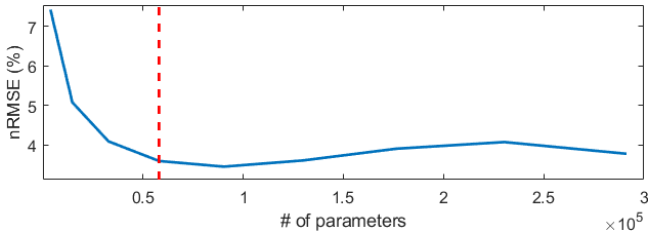

Fig. 1: Number of parameters versus nRMSE for the proposed SR architecture on the validation set. Red dashed line marks the 58,000 point.

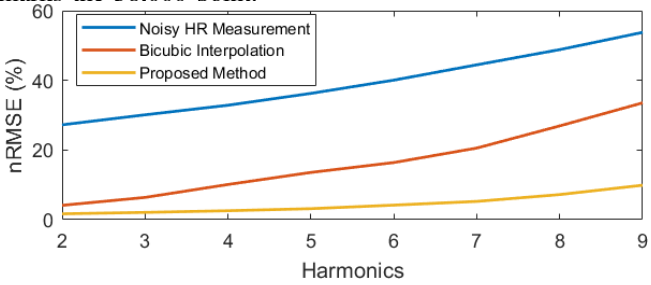

Fig. 2: nRMSE per harmonics frequency for the proposed SR architecture on the test set.

a canonical L-curve is observed, with the elbow point near 58,000 parameters with an optimal growth rate of 4.

Next, we compared the performance of SM estimation using the proposed method, bicubic interpolation and performing a HR SM calibration (that is noisy and elicits a 16-fold increase in scan time). Figure 2 shows estimation performance in the test set across harmonics. As expected, nRMSE is elevated towards higher harmonics for all methods, but the increases are relatively modest for the proposed method. Noisy HR measurement only suffers from the decrease in the SNR, while other methods also have to infer complex structures at higher harmonics without corresponding measurements. Furthermore, the proposed method outperforms the two other methods. Hence, it is especially advantageous to use proposed method for higher harmonics that bears high-resolution information.

Lastly, we examine the effects of SM estimation on the subsequent image reconstruction task. Here, we compared the performance of the proposed method ($\mathbf{A}_{prop}$) with LR SM ($\mathbf{A}_{LR}$), HR SM ($\mathbf{A}_{HR}$), noiseless HR SM ($\mathbf{A}_{ref}$) and bicubic interpolated SM ($\mathbf{A}_{int}$). Next, we simulated some image phantoms that demonstrate the resolution and contrast. We first constructed an imaging phantom ($\mathbf{x}_{ref}$), and simulated the output data using $\mathbf{A}_{ref}\mathbf{x}_{ref}$ and added white Gaussian noise. We finally reconstructed images using the generated data and compared the images reconstructed using different SMs. Figure 3 shows the reconstructed images for different SMs under 30 dB data SNR. Reconstruction based on noiseless HR SM reflect an upper limit for calibration and reconstruction performance. Reconstruction based on noisy HR measurements yield poor results due to limited SNR despite the 16-fold longer calibration time. Reconstruction based on LR SM naturally lead to loss of image details. While bicubic interpolation SM improves recon quality, it suffers from loss of high-spatial frequency details. In

SNR	$\mathbf{A}_{ref}$	$\mathbf{A}_{HR}$	$\mathbf{A}_{LR}$	$\mathbf{A}_{int}$	$\mathbf{A}_{prop}$
10	16.38 0.64	15.92 0.57	15.26 0.48	14.97 0.44	16.36 0.64
20	18.74 0.77	15.37 0.54	15.39 0.49	14.86 0.43	18.94 0.78
30	21.45 0.82	17.22 0.71	15.40 0.49	14.98 0.45	22.33 0.88

TABLE I: Average pSNR and (SSIM) values of reconstructed images under various SNR settings.

contrast, the proposed method yields superior reconstructions that are on par with the those based on noiseless HR SM. Broader comparisons at multiple SNR levels averaged over 150 Monte Carlo runs are summarized in Table I. As can be seen, the proposed method consistently outperforms other methods in terms of pSNR and SSIM. The distinction becomes clearer as SNR increases.

V. Discussion

In this study, we introduced a learning-based method for acquiring high-resolution SM within short calibration times in MPI. The proposed method uses a deep CNN model to jointly superresolve and denoise SM. MPI images have small sizes compared to natural images. For this purpose, we designed a compact network architecture with an order-of-magnitude fewer parameters compared to vanilla CNN models in computer vision. To account for complex MPI data, real and imaginary components of SM rows were processed separately. Our experiments demonstrate clearly that the proposed method outperforms conventional low-resolution SM acquisition and bicubic interpolation in both SM estimation and image reconstruction. Therefore, the proposed method holds promise for improving calibration efficiency and utility of MPI.

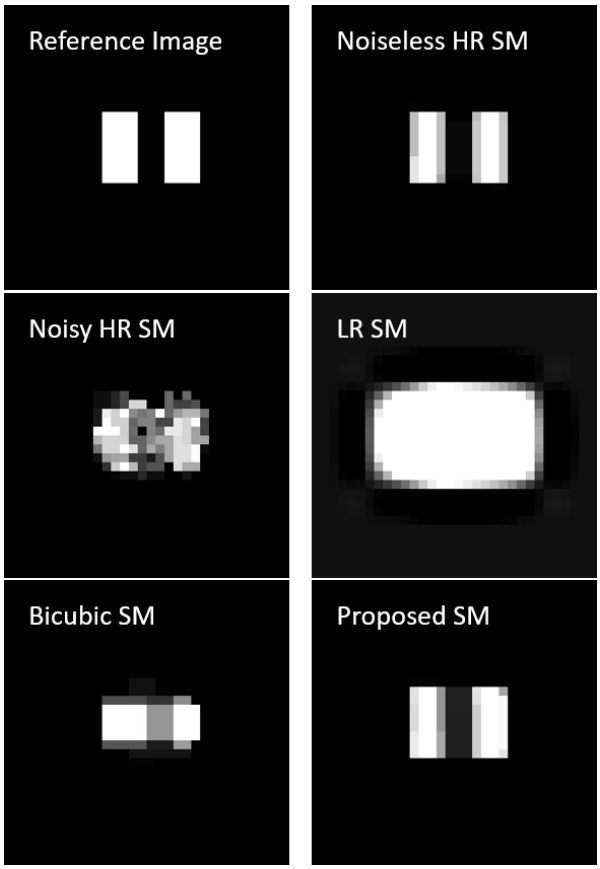

Fig. 3: Reference image (top left), Reconstruction using noiseless SM (top right, upper performance limit), noisy HR SM (middle left), LR SM (middle right), bicubic interpolated SM (bottom left), proposed method (bottom right).

References

[1] B. Gleich and J. Weizenecker, "Tomographic imaging using the nonlinear response of magnetic particles," *Nature*, vol. 435, no. 7046, pp. 1214–1217, 2005.

[2] J. Weizenecker, B. Gleich, J. Rahmer, H. Dahnke, and J. Borgert, "Three dimensional real time in vivo magnetic particle imaging," *Phys. Med. Biol*, vol. 54, no. 5, pp. L1–L10, feb 2009.

[3] B. Zheng, T. Vazin, P. W. Goodwill, A. Conway, A. Verma, E. U. Saritas, D. Schaffer, and S. M. Conolly, "Magnetic particle imaging tracks the long-term fate of in vivo neural cell implants with high image contrast," *Scientific reports*, vol. 5, no. 1, pp. 1–9, 2015.

[4] X. Zhang, T.-A. Le, and J. Yoon, "Development of a real time imaging-based guidance system of magnetic nanoparticles for targeted drug delivery," *J. Magn. Magn. Mater.*, vol. 427, pp. 345–351, 2017.

[5] J. R. McCarthy and R. Weissleder, "Multifunctional magnetic nanoparticles for targeted imaging and therapy," *Adv. Drug Deliv. Rev.*, vol. 60, no. 11, pp. 1241–1251, 2008.

[6] S. Ilbey, C. B. Top, A. Güngör, T. Çukur, E. U. Saritas, and H. E. Güven, "Comparison of system-matrix-based and projection-based reconstructions for field free line magnetic particle imaging," *International J. on Magn. Par. Imag.*, vol. 3, no. 1, 2017.

[7] A. Von Gladiss, M. Gräser, P. Szwargulski, T. Knopp, and T. M. Buzug, "Hybrid system calibration for multidimensional magnetic particle imaging," *Phys. Med. Biol.*, vol. 62, no. 9, p. 3392, 2017.

[8] T. Knopp and T. M. Buzug, *Magnetic particle imaging: An introduction to imaging principles and scanner instrumentation*. Springer Science & Business Media, 2012.

[9] J. Lampe, C. Bassoy, J. Rahmer, J. Weizenecker, H. Voss, B. Gleich, and J. Borgert, "Fast reconstruction in magnetic particle imaging," in *Physics in Medicine and Biology*, vol. 57, no. 4. IOP Publishing, feb 2012, pp. 1113–1134.

[10] A. Weber and T. Knopp, "Reconstruction of the magnetic particle imaging system matrix using symmetries and compressed sensing," in *Advances in Mathematical Physics*. Hindawi Publishing Corporation, oct 2015, pp. 1687–9120.

[11] S. Ilbey, C. B. Top, A. Güngör, T. Çukur, E. U. Saritas, and H. E. Güven, "Fast system calibration with coded calibration scenes for magnetic particle imaging," *IEEE Trans Med Imaging*, vol. 38, no. 9, pp. 2070–2080, 2019.

[12] T. Kluth, C. Bathke, M. Jiang, and P. Maass, "Joint super-resolution image reconstruction and parameter identification in imaging operator: analysis of bilinear operator equations, numerical solution, and application to magnetic particle imaging," *Inverse Problems*, vol. 36, no. 12, p. 124006, dec 2020.

[13] C. Ledig, L. Theis, F. Huszár, J. Caballero, A. Cunningham, A. Acosta, A. Aitken, A. Tejani, J. Totz, Z. Wang, and W. Shi, "Photo-realistic single image super-resolution using a generative adversarial network," in *2017 IEEE Conference on Computer Vision and Pattern Recognition (CVPR)*, 2017, pp. 105–114.

[14] J. W. Soh, G. Y. Park, J. Jo, and N. I. Cho, "Natural and realistic single image super-resolution with explicit natural manifold discrimination," in *2019 IEEE/CVF Conference on Computer Vision and Pattern Recognition (CVPR)*, 2019, pp. 8114–8123.

[15] Y. Zhang, Y. Tian, Y. Kong, B. Zhong, and Y. Fu, "Residual dense network for image super-resolution," in *2018 IEEE/CVF Conference on Computer Vision and Pattern Recognition*, 2018, pp. 2472–2481.

[16] A. Gungor and C. B. Top, "Super-resolving reconstruction technique for mpi," *International J. on Magn. Par. Imag.*, vol. 6, no. 2, 2020.

[17] C. B. Top and A. Güngör, "Tomographic field free line magnetic particle imaging with an open-sided scanner configuration," *IEEE Trans Med Imaging*, vol. 39, no. 12, pp. 4164–4173, 2020.

[18] S. Chikazumi and S. H. Charap, *Physics of magnetism*. Wiley, New York, 1964.